

Calculations of the Structure of Basin Volumes for Mechanically Stable Packings

S. S. Ashwin^{1,2}, Jerzy Blawdziewicz³, Corey S. O'Hern^{1,2}, and Mark D. Shattuck⁴

¹ *Department of Mechanical Engineering and Materials Science, Yale University, New Haven, CT 06520-8286*

² *Department of Physics, Yale University, New Haven, CT 06520-8120*

³ *Department of Mechanical Engineering, Texas Tech University, Lubbock, TX 74909-1021 and*

⁴ *Benjamin Levich Institute and Physics Department,*

The City College of the City University of New York, New York, NY 10031

(Dated: August 2, 2021)

There are a finite number of distinct mechanically stable (MS) packings in model granular systems composed of frictionless spherical grains. For typical packing-generation protocols employed in experimental and numerical studies, the probabilities with which the MS packings occur are highly nonuniform and depend strongly on parameters in the protocol. Despite intense work, it is extremely difficult to predict *a priori* the MS packing probabilities, or even which MS packings will be the most versus the least probable. We describe a novel computational method for calculating the MS packing probabilities by directly measuring the volume of the MS packing ‘basin of attraction’, which we define as the collection of initial points in configuration space at *zero packing fraction* that map to a given MS packing by following a particular dynamics in the density landscape. We show that there is a small core region with volume V_n^c surrounding each MS packing n in configuration space in which all initial conditions map to a given MS packing. However, we find that the MS packing probabilities are very weakly correlated with core volumes. Instead, MS packing probabilities obtained using initially dilute configurations are determined by complex geometric features of the basin of attraction that are distant from the MS packing.

PACS numbers: 63.50.Lm, 83.80.Fg, 61.43.-j, 64.70.ps

I. INTRODUCTION

In contrast to equilibrium, thermal systems, the structural and mechanical properties of dense granular materials and other athermal particulate systems depend strongly on the protocol used to create them. For example, a number of studies have shown that the packing fraction of granular assemblies can vary from values associated with random loose [1] to random close packing [2] as a function of the vibration amplitude and tapping history [3, 4]. In addition, the force chain networks that form, and thus the shear modulus of granular packings depend on whether they have been generated via shear, isotropic compression [5], or sedimentation via single-particle or collective deposition [6].

The protocol dependence in dense granular systems arises from the nonlinear, dissipative, and frictional contact interactions between grains [7]. Despite active research in this area, the distinct contributions from each of these interactions to protocol dependence has not been determined. In this manuscript, we will investigate the protocol-dependence of static granular packings by focusing on a simple system of frictionless spherical particles that interact via purely repulsive linear spring and velocity-dependent damping forces. For a fixed set of boundary conditions, there are finite number of distinct mechanically stable (MS) packings of frictionless particles, which grows exponentially with the number of particles N [8]. MS packings exist as discrete points in configuration space that are characterized by the packing fraction ϕ_J and N particle coordinates $\vec{R}_J = \{\vec{r}_1, \vec{r}_2 \dots \vec{r}_N\}$ and coincide with local minima of the density landscape [9, 10] (or local minima of the potential energy

landscape with zero potential $V = 0$). We have shown recently in both simulations and experiments that the probabilities with which these distinct MS packings occur are highly nonuniform and depend on parameters of the packing-generation protocol including the compression rate, damping coefficient, and initial packing fraction [11, 12]. However, one cannot yet determine *a priori* which MS packings are the most versus the least probable, much less calculate the packing probabilities as a function of the packing-generation protocol.

Here we describe a novel computational method for calculating the MS packing probabilities by directly measuring the volume of the MS packing ‘basin of attraction’, which we define as the collection of initial points in configuration space (*i.e.*, the red region in Fig. 1) at *zero packing fraction* that map to a given MS packing by following a particular dynamics in the density landscape. Note that our definition of the basin of attraction is protocol-dependent, and thus the basin volume will vary with the rate at which energy is dissipated, the compression rate, and other parameters. In contrast, basins of attraction for glassy systems [13, 14] are defined as the set of initial dense liquid configurations that map to the ‘nearest’ local minimum using steepest descent dynamics at fixed density. Our definition of basin volumes is more relevant for granular systems, in which MS packings are generated from initially dilute configurations.

To aid in the calculation of the basin volumes, we introduce the unweighted basin profile function $f_n^\Gamma(l)$, which is the fraction of points on a hypersurface in configuration space a distance l from the n th MS packing that maps via a given dynamics (labeled Γ) to MS packing n . We will show that there is a hyperspherical core region surround-

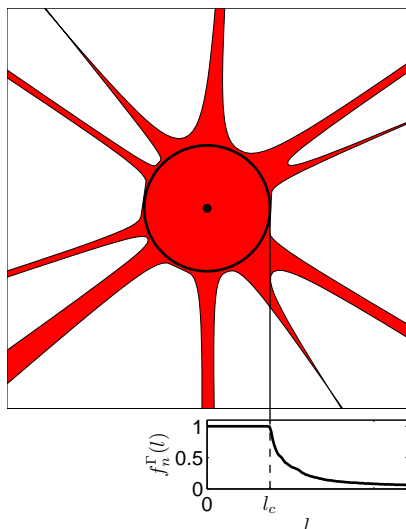


FIG. 1: (color online) (top) A schematic of the basin of attraction (red) in dN -dimensional configuration space for a typical mechanically stable (MS) packing (black dot). (bottom) The corresponding unweighted basin profile function $f_n^\Gamma(l)$ is plotted as a function of distance l from MS packing n for packing-generation protocol Γ . $f_n^\Gamma(l)$ begins to decay from 1 beyond an approximately spherically symmetric core size l_c , while for $l > l_c$ the basin is highly branched, thread-like, and $f_n^\Gamma(l) \rightarrow 0$.

ing each MS packing in which $f_n^\Gamma(l) = 1$ for $l < l_c$, while further from the MS packing, the basin becomes highly branched, thread-like, and $f_n^\Gamma(l) \rightarrow 0$. (See Fig. 1.) This picture raises several key questions: 1) Are the MS packing probabilities determined by the size l_c of the core region in configuration space or dominated by contributions from the thread-like regions, and 2) do the morphologies of the basins of attraction depend sensitively on protocol? We will show below that the MS packing probabilities are not strongly correlated with the volume of the core regions in configuration space and are instead determined by features of the density landscape that are far from each MS packing packing. Thus, novel computational geometry techniques [15] must be developed to understand the key features of configuration space that control MS packing probabilities.

II. METHODS

To perform our calculations of basin volumes, we focused on a well-characterized model system composed of N frictionless disks in 2D that interact via purely repulsive linear spring and velocity-dependent damping forces. N is varied from 3 to 100, and the particles are enclosed in a square cell with fixed walls of length $L = 1$. Interactions with the walls match those between the particles. We consider both monodisperse and bidisperse systems, where the bidisperse mixtures contain half large and half small disks ($N_s = N_l = N/2$) with diameter ratio $\sigma_l/\sigma_s = 1.4$.

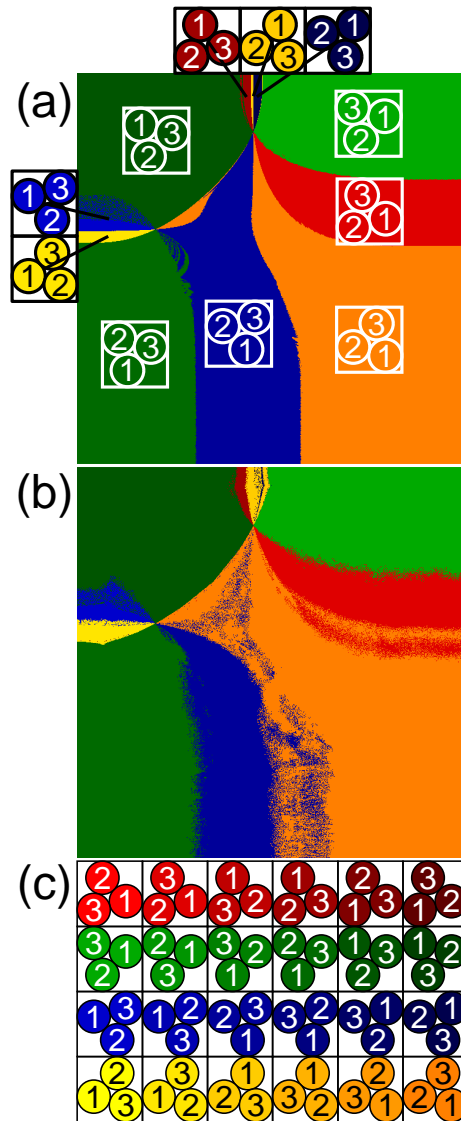


FIG. 2: (color online) The microstate basins of attraction for a system of three monodisperse frictionless disks, where particles 2 and 3 are initially located at positions $(0.2, 0.6)$ and $(0.45, 0.85)$ in the x - y plane (with the origin in the lower left corner). Results are shown for two damping coefficients, (a) $\tilde{b} = 1$ and (b) $\tilde{b} = 0.1$. The position of each pixel represents the initial position of particle 1 and its color corresponds to one of the 11 out of 24 microstates in (c) to which the system evolved under the compression protocol. For $N = 3$ monodisperse systems, there is one distinct MS packing ($\mathcal{N}_s = 1$) with four polarizations (hue; rows) and six permutations (saturation; columns) for a total of $\mathcal{N}_m = 24$ microstates.

In a number of previous studies, we described the MS ‘packing finder’ that generates a mechanically stable packing via isotropic compression at ϕ_J with infinitesimal overlap from an arbitrary initial condition at $\phi = 0$ [11]. Briefly, the algorithm includes the following steps. For each trial, we initialize the system with random particle positions inside the unit square at $\phi = 0$ and zero veloci-

N	\mathcal{N}_s	\mathcal{N}_m
2	1	4
3	1	24
4	6	136
6	80	19440
12	~ 12000	$\sim 4 \times 10^{10}$

TABLE I: The number of distinct mechanically stable packings \mathcal{N}_s and total number of microstates \mathcal{N}_m versus the number of particles N . For $N = 3$ we consider monodisperse systems. For the other system sizes, results are given for bidisperse mixtures. For $N = 12$ we estimate \mathcal{N}_s and \mathcal{N}_m . We do not include unstable packings such as the one in the upper left corner of Fig. 3 in which the ‘rigid backbone’ of particles can translate.

ties. We then compress the system in steps of $\Delta\phi = 10^{-4}$ and relax the small particle overlaps after each step by solving Newton’s equations of motion with damping,

$$m\vec{a}_i = \sum_j \vec{F}(r_{ij}) - b\vec{v}_i, \quad (1)$$

where m , σ , and \vec{a}_i are the particle mass, diameter, and acceleration,

$$\vec{F}(r_{ij}) = \frac{\epsilon}{\sigma} \left(1 - \frac{r_{ij}}{\sigma}\right) \Theta\left(1 - \frac{r_{ij}}{\sigma}\right) \hat{r}_{ij}, \quad (2)$$

ϵ is the characteristic energy of the repulsive spring interaction, $\Theta(x)$ is the Heaviside step function, $\tilde{b} = b\sigma/\sqrt{m\epsilon}$ is the damping coefficient, \hat{r}_{ij} is the unit vector connecting the centers of particles i and j and r_{ij} is their separation, until the kinetic energy per particle falls below a specified tolerance $K/\epsilon N < K_{\text{tol}} = 10^{-25}$. We studied a wide range of values for the damping coefficient from $\tilde{b} = 10^{-2}$ to 10, which mimics steepest descent dynamics. The packing-generation algorithm terminates when the minimized total potential energy per particle $V/\epsilon N > V_{\text{tol}} = 10^{-16}$. As in previous studies on similar systems with periodic boundary conditions, we distinguish MS packings based on the spectrum of nontrivial eigenvalues of the dynamical matrix [12], and we find that the number of distinct MS packings \mathcal{N}_s grows exponentially with N as shown in Table I. The $\mathcal{N}_s = 6$ and 80 distinct MS packings for $N = 4$ and 6 are shown in Figs. 3 and 4. The packing finder does produce a small number of unstable packings as shown in Fig. 3, but these are not included in the analyses.

The fundamental quantity in our approach is the unweighted basin profile function $f_n^\Gamma(l)$ defined as

$$f_n^\Gamma(l) = \int d\vec{R} G_\Gamma(\vec{R}, \vec{R}_j^n) \delta(|\vec{R} - \vec{R}_j^n| - l), \quad (3)$$

where $f_n^\Gamma(l)$ is sampled on hyperspherical shells a distance l from MS packing n , Γ is the specified compression dynamics, $\delta(x)$ is the Dirac delta function, $G_\Gamma(\vec{R}, \vec{R}_j^n) = 1$ for points \vec{R} in configuration space that map to MS packing \vec{R}_j^n , and 0 otherwise. As an illustrative example,

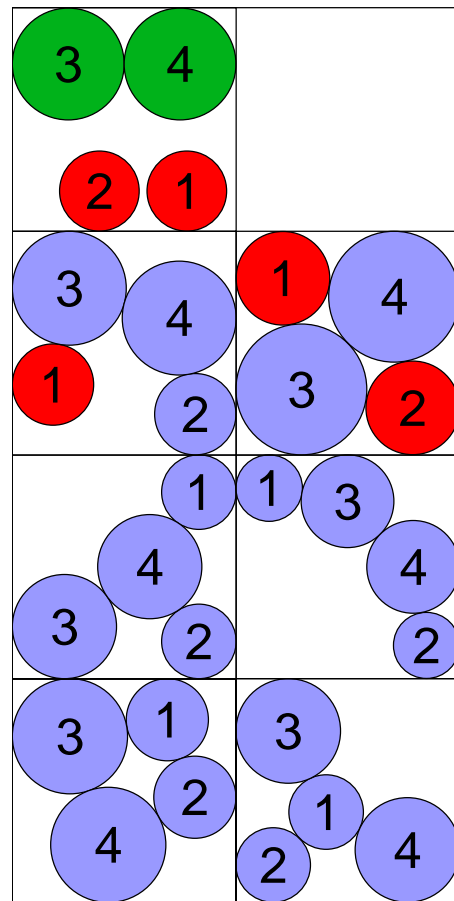


FIG. 3: (color online) The bottom six configurations are the $\mathcal{N}_s = 6$ distinct mechanically stable packings for bidisperse systems with $N = 4$. (We will refer to configurations 1 through 6 counting in ascending order from left to right and bottom to top.) The particles shaded blue form the force-bearing backbone of the mechanically stable packing. Particles shaded red are ‘rattlers’ with fewer than 3 contacts. The packing finder generates a small number of unstable configurations similar to that shown in the upper left corner with probability less than 0.2%, but these are not included in the analyses.

we calculate slices of $G_\Gamma(\vec{R}, \vec{R}_j^n)$ for $N = 3$, which has a single MS packing with \mathcal{N}_m microstates—6 particle-label permutations and 4 polarizations obtained by applying all possible reflections and rotations in 2D consistent with the square cell boundary conditions [16]. In Fig. 2, we plot the microstate basins of the attraction $\sum_{n=1}^{\mathcal{N}_m} nG(\{\vec{r}_1, \vec{r}_2^0, \vec{r}_3^0\}, \vec{R}_j^n)$ for fixed $\vec{r}_2^0 = (0.2, 0.6)$ and $\vec{r}_3^0 = (0.45, 0.85)$.

We calculate the unweighted basin profile function $f_n^\Gamma(l)$ using two procedures; the first method is efficient and accurate for small l and the second for large l . For method 1, we generate at least $M = 10^6$ points randomly on the surface of a $2N$ -dimensional hypersphere centered on the MS packing with radius l . We then input each of these configurations as initial configurations

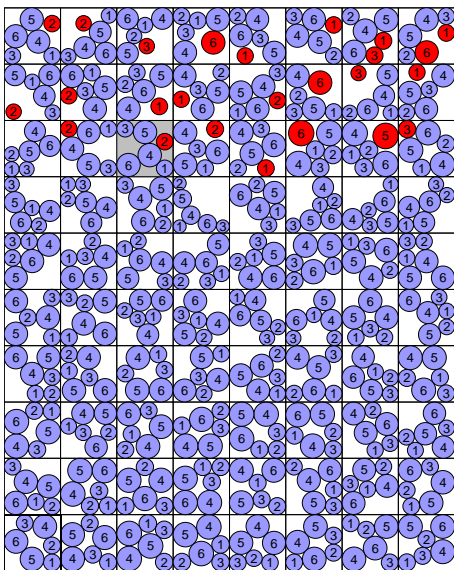


FIG. 4: (color online) The $\mathcal{N}_s = 80$ distinct mechanically stable packings for bidisperse systems with $N = 6$. The particles shaded blue form the force-bearing backbone of the mechanically stable packing. Particles shaded red are ‘rattlers’ with fewer than 3 contacts. The unweighted and weighted basin profile functions are shown in Fig. 11 for the configuration in the third row that is shaded gray.

into the MS packing finder with packing fraction $\phi_i = 0$. If a given initial condition belongs to the basin of attraction of MS packing n , the packing finder will generate packing n . Otherwise, the initial condition belongs to a different basin. For the system sizes where we can achieve complete enumeration, we found that the criterion, $\max_i (d_i^j - d_i^k) / d_i^k < 10^{-6}$, was sufficiently sensitive to distinguish MS packings, where d_i^j is the i th sorted eigenvalue of the dynamical matrix for MS packing j . From method 1, the unweighted basin profile function for MS packing n is

$$f_n^\Gamma(l) = \frac{M_n}{M}, \quad (4)$$

where M_n is the number of initial conditions at l that map to packing n .

We define the basin volume for MS packing n generated using compression dynamics Γ as

$$V_n = \int_0^{\sqrt{2N}} S_n^\Gamma(l) dl, \quad (5)$$

where

$$S_n^\Gamma(l) = A_{2N} f_n^\Gamma(l) l^{2N-1} \mathcal{P}_n N_s! N_l! \quad (6)$$

is the (angle-averaged) weighted basin profile function, $A_k = 2\pi^{k/2} / \Gamma(k/2)$ is the surface area of a k -dimensional unit sphere, and \mathcal{P}_n is the number of distinct polarizations for MS packing n [16]. The probability of MS

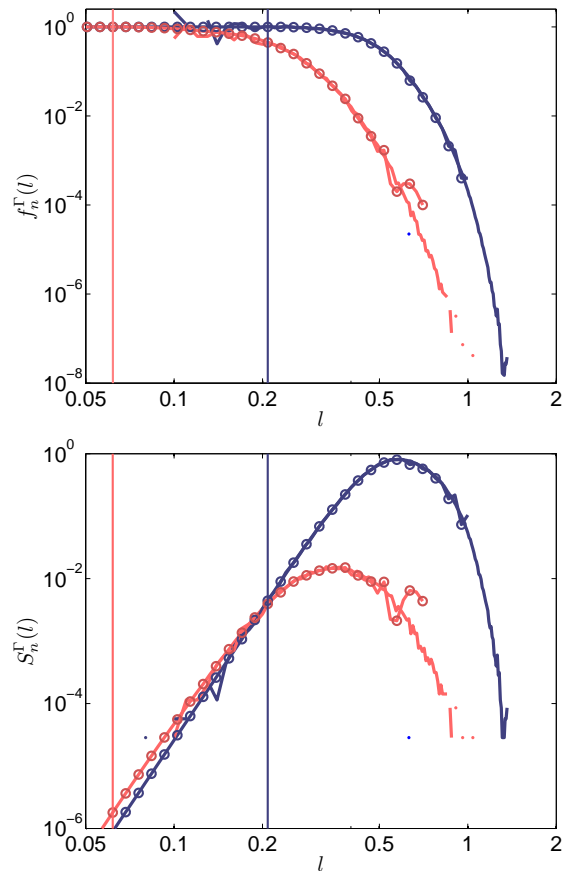


FIG. 5: (color online) [top] The unweighted $f_n^\Gamma(l)$ and [bottom] weighted $S_n^\Gamma(l)$ basin profile functions measured using methods 1 (circles) and 2 (solid lines) for MS packings 1 (highest probability; dark blue line) and 4 (lowest probability; light red line) shown in Fig. 3 plotted on a log-log scale for $N = 4$ and $\bar{b} = 1$. The vertical lines indicate l_c for each MS packing.

packing n for a given compression protocol Γ is proportional to its basin volume, $P_n^\Gamma = V_n^\Gamma / V_{\text{tot}}^\Gamma$, where $V_{\text{tot}}^\Gamma = \sum_{n=1}^{\mathcal{N}_s} V_n^\Gamma = L^{2N} = 1$.

Method 1 becomes extremely inefficient at calculating $f_n^\Gamma(l)$ for large $l > l_c$. Thus, in this regime we implement method 2, which was previously employed to calculate the probabilities P_n^Γ directly [8]. For this method, we generate at least 10^6 random points in configuration space and input these into the packing finder with $\phi_i = 0$. The fraction of random initial configurations that map to MS packing n determines P_n^Γ . We can then calculate $f_n^\Gamma(l)$ from P_n^Γ using Eqs. 5 and 6. Note that an advantage of method 2 is that each initial condition provides information about P_n^Γ for some n and for $N_s! N_l!$ distances l by permuting the labels of the final MS packing.

III. RESULTS

Typical basin profile functions $f_n^\Gamma(l)$ are shown for the most and least probable MS packings (1 and 4 in Fig. 3)

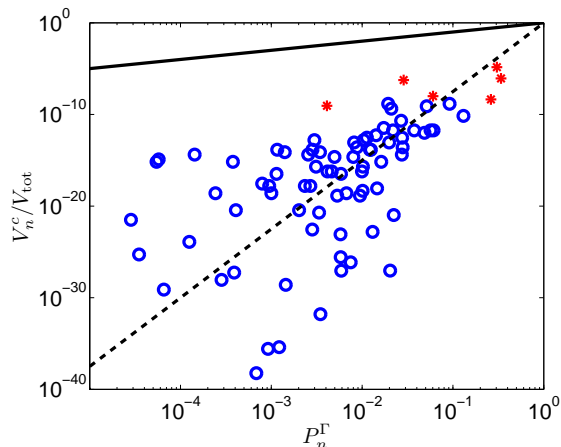


FIG. 6: The volume V_n^c of the hyperspherical cores surrounding each MS packing n (relative to V_{tot}) plotted as a function of the MS packing probability P_n^Γ for each MS packing for $N = 4$ (asterisks) and 6 (circles) obtained using method 1 with damping parameter $\tilde{b} = 1$. The solid (dashed) line has slope 1 (7.5).

for $N = 4$ in the top panel of Fig. 5. For small distances from the MS packing $l < l_c$, $f_n(l) = 1$. Beyond the core size l_c , which can vary strongly from one MS packing to another, $f_n^\Gamma(l)$ decays rapidly to zero. In the bottom panel of Fig. 5, we show the weighted basin profile $S_n^\Gamma(l)$ for the same $N = 4$ MS packings. Since $S_n^\Gamma(l)$ is obtained by multiplying $f_n^\Gamma(l)$ by l^{2N-1} , the probabilities for obtaining MS packings (when starting from zero packing fraction) are determined by distances $l > l_c$. For $N = 4$ the average core size is $\langle l_c \rangle \approx 0.1$, the small particle diameter is $\sigma = 0.3$, but the average length scale that yields 50% of the packing probabilities (near the peak in $S_n^\Gamma(l)$) is $\langle l_p \rangle \approx 0.5$. We will show below that l_p grows with increasing system size. We have validated the results by ensuring that methods 1 and 2 yield the same values for $f_n^\Gamma(l)$ and $S_n^\Gamma(l)$ over the range in l in which the calculations overlap.

In the top panel of Fig. 5, we show that the core size for the most probable $N = 4$ MS packing is larger than that for the least probable MS packing, which may suggest that there is a correlation between the core size and the MS packing probabilities. To investigate to what extent the hyperspherical core surrounding each MS packing determines the packing probabilities, we approximate the basin volume by the volume of a hypersphere of radius l_c , $V_n^c = \pi^N l_c^{2N} / \Gamma(N + 1)$, for each MS packing. In Fig. 6, we plot V_n^c / V_{tot} versus P_n^Γ for $N = 4$ and 6. We find two key results: 1) The volumes V_n^c / V_{tot} are smaller by many orders of magnitude than the probabilities P_n^Γ and 2) A fit to the data for $N = 6$ yields $V_n^c / V_{\text{tot}} \sim (P_n^\Gamma)^\lambda$ with $\lambda \approx 7.5$, but there is only a very weak correlation between V_n^c / V_{tot} and the packing probabilities. For example, the scatter in the data can vary by more than 20 orders of magnitude! Thus, features of the basin geometrical structure beyond the core region control the

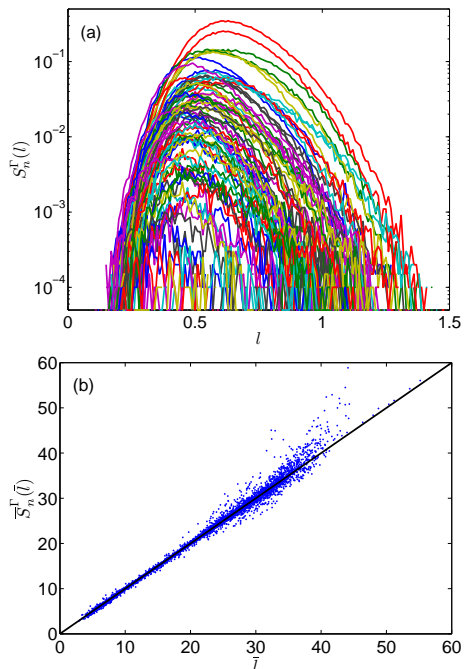


FIG. 7: (a) The weighted basin profile functions $S_n^\Gamma(l)$ (for each of the $\mathcal{N}_s = 80$ distinct MS packings for $N = 6$) sampled on hyper-spherical shells a distance l from MS packing n using method 2 with $\tilde{b} = 1$. (b) The scaled weighted basin profile function $\bar{S}_n^\Gamma(\bar{l}) = [S_n^\Gamma(l)\theta\Gamma(k)e^{-l/\theta}]^{1/(k-1)}$ plotted versus the scaled distance $\bar{l} = l/\theta$ for the same data in (a). The solid line has slope 1.

MS packing probabilities for packings that are generated from dilute initial configurations.

To begin to investigate the nature of the basin morphology beyond the core region, we characterize in detail the shapes of the weighted basin profile functions for each of the \mathcal{N}_s MS packings for $N = 6$ in Fig. 7 (a). As found for the distribution of Voronoi volumes in dense granular packings [17–19], the form of $S_n^\Gamma(l)$ is described by a Γ -distribution

$$S_n^\Gamma(l) = \frac{\left(\frac{l}{\theta}\right)^{k-1} e^{-l/\theta}}{\theta\Gamma(k)}, \quad (7)$$

where $\theta = (\langle l^2 \rangle - \langle l \rangle^2) / \langle l \rangle$, $k = \langle l \rangle / \theta$, and $\langle l \rangle = \int_0^\infty dl l S_n^\Gamma(l)$. The scaled weighted basin profile functions $\bar{S}_n^\Gamma(\bar{l}) = [S_n^\Gamma(l)\theta\Gamma(k)e^{-l/\theta}]^{1/(k-1)}$ for all microstates collapse when plotted versus the scaled distance $\bar{l} = l/\theta$. The wider scatter at large \bar{l} is caused by under sampling low probability configurations. We find similar quality for the collapse at larger N .

We investigate the system size dependence of the average weighted basin profile function

$$S^\Gamma(l) = \sum_{n=1}^{\mathcal{N}_s} P_n^\Gamma S_n^\Gamma(l) \quad (8)$$

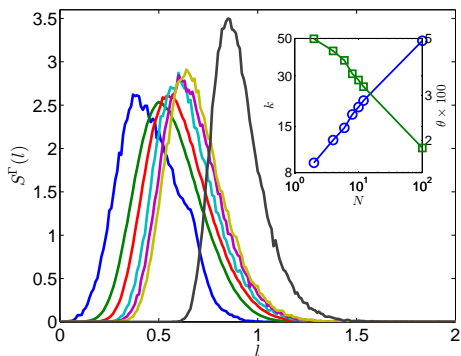


FIG. 8: The average weighted basin profile function $S^\Gamma(l)$ for several system sizes $N = 2, 4, 6, 8, 10, 12,$ and 100 (from left to right) for damping parameter $\tilde{b} = 1$. The inset shows the parameters k (circles; left axis) and 100θ (squares; right axis) that describe fits of $S^\Gamma(l)$ to the Γ -distribution (Eq. 7) versus N on a log-log scale.

in Fig. 8 over the range $N = 2$ to 100 . $S^\Gamma(l)$ shifts to larger l with increasing N ; the peak position k increases by a factor of 5 and scales roughly as \sqrt{N} over this range in N . The width θ slightly narrows over the same range of N , scaling roughly as $N^{-1/4}$.

We also investigated the protocol dependence of the basin profile functions by varying the damping parameter (\tilde{b} in Eq. 1) used in the packing finder in method 2. Lowering \tilde{b} decreases the rate at which energy is removed from the system and allows the system to explore larger regions of configuration space. In contrast, larger \tilde{b} increases the rate at which energy is removed from the system, and thus the initial configurations are typically closer to the final MS packings. In the top panel of Fig. 9, we plot the average weighted basin profile function versus the damping parameter employed in method 2 over three orders of magnitude in \tilde{b} from 10^{-2} to 10 . We were able to saturate the \tilde{b} dependence of $S^\Gamma(l)$ for both large and small \tilde{b} , *i.e.* for $\tilde{b} < 10^{-2}$ and $\tilde{b} > 10$, $S^\Gamma(l)$ is very weakly dependent on \tilde{b} . The two parameters k and θ that describe the shape of $S^\Gamma(l)$ exhibit two key features in the bottom panel of Fig. 9: 1) the peak of the distribution (captured by k) and thus the lengthscales that determine the MS packing probabilities increase with decreasing \tilde{b} and 2) the variance (relative to the average) depends weakly on \tilde{b} , but does possess a small peak near $\tilde{b} = 10^{-1}$. We expect that the qualitative features of the \tilde{b} dependence will persist for larger system sizes. In future studies, we will predict the locations of the peaks in $S^\Gamma(l)$ at large and small \tilde{b} by calculating the distances between random points in configuration space and between random points and configurations related by particle label permutations, respectively.

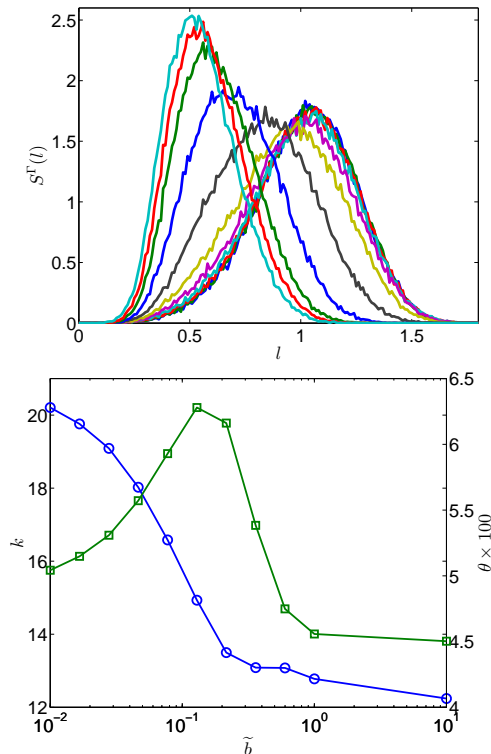


FIG. 9: [top] The average weighted basin profile function $S^\Gamma(l)$ for $N = 4$ plotted over a wide range of the damping coefficients \tilde{b} employed in method 2. \tilde{b} ranges from 0.01 to 10 from left to right. [bottom] The parameters k (circles; left axis) and 100θ (squares; right axis) that describe fits of $S^\Gamma(l)$ in (a) to the Γ -distribution (Eq. 7) versus \tilde{b} .

IV. CONCLUSIONS

In this manuscript, we described and carried out a novel computational method for calculating the volume of the MS packing ‘basins of attraction’, which we define as the collection of initial points in configuration space at *zero packing fraction* that map to a given MS packing by following a particular dynamics in the density landscape. Note that our definition of the basin of attraction is protocol-dependent, and thus the basin volume will vary with the rate at which energy is dissipated, the compression rate, and other parameters. Using dilute configurations as initial conditions and including variations in the basin volume with changes in the packing-generation protocol are crucial for understanding the protocol-dependent structural and mechanical properties of granular media and other athermal particulate systems.

Our computational studies of the basin volumes have uncovered three important results: 1) A small approximately hyperspherical region of the basin of attraction with radius l_c surrounds each MS packing, but the volume of this region (relative to V_{tot}) is much smaller and only very weakly correlated with the MS packing prob-

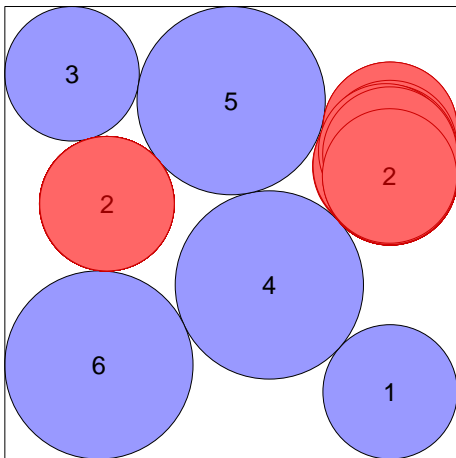


FIG. 10: 113 snapshots of one of the $N = 6$ mechanically stable packings (shaded gray in Fig. 4) generated from independent random initial conditions. This packing contains one rattler particle (labeled 2) that can be positioned in the cavity on the left or right and at multiple positions in the right cavity.

abilities in contrast to previous studies of jammed systems [14]; 2) the probabilities of MS packings initialized with dilute configurations are instead controlled by features of the basins of attraction at lengthscales much further from the MS packing than the core region. In addition, the lengthscales that control the MS packing probabilities grow with increasing system size and decreasing damping parameter \tilde{b} ; and 3) The shape of the basin profile functions are well characterized by a Γ distribution, which suggests that we can construct a statistical mechanics-like theory to predict the shape of $S^\Gamma(l)$ and the MS packing probabilities.

Acknowledgments This research was supported by the National Science Foundation under Grant Nos. CBET-0967262 (SA, JB, CO) and CBET-0968013 (SA, MS).

Appendix A: Rattler Particles

As shown in Figs. 3 and 4, MS packings contain rattler particles. Two of the $\mathcal{N}_s = 6$ distinct MS packings for $N = 4$ and 24 of the $\mathcal{N}_s = 80$ distinct MS packings for $N = 6$ contain rattler particles. For these small- N systems, the fraction of MS packings that contain rattlers is larger than the fraction of particles (roughly 5%-10%) that are rattlers in large MS packings [20], but these results suggest that the number of MS packings containing rattlers is extensive with \mathcal{N}_s [21]. How do rattler particles affect the calculation of the basins of attraction for MS packings?

We find that the correspondence between the unweighted $f_n^\Gamma(l)$ and weighted $S_n^\Gamma(l)$ basin profile functions breaks down for small l for MS packings that contain

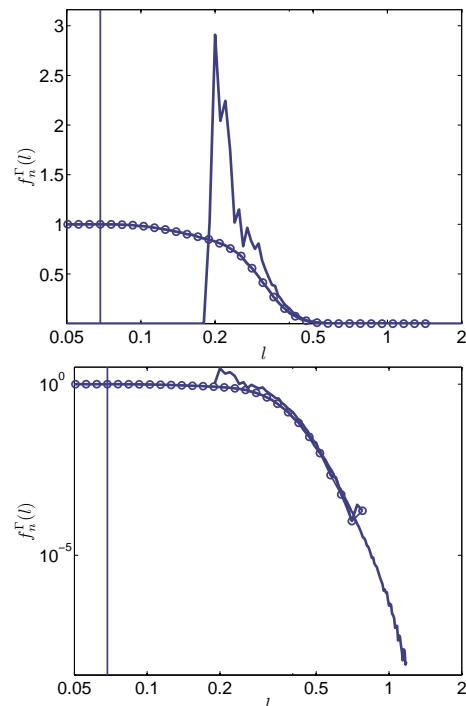


FIG. 11: (color online) The basin profile function $f_n^\Gamma(l)$ on linear-log [top] and log-log [bottom] scales measured using methods 1 (circles) and 2 (solid lines) for the MS packing in Fig. 10 for $\tilde{b} = 1$. The vertical lines indicate l_c .

rattler particles. As shown in Fig. 10, for MS packings containing rattlers it is difficult to define uniquely the distance from the initial state to the final MS packing because the rattler particle can exist over a range of positions for a given distinct MS packing. Further, the different rattler locations may give widely varying contributions to the MS packing probability.

In Fig. 11, we plot $f_n^\Gamma(l)$ calculated using methods 1 (circles) and 2 (solid lines) for the MS packing depicted in Fig. 10. As described in Sec. III, for method 1, we measure the fraction of times the system returns to the initial MS packing after a perturbation of size l , which is largely unaffected by the presence of rattlers. For method 2, we measure the normalized distribution of distances between the initial configurations and the final MS packings. For large l , method 2 is also largely unaffected by the presence of rattlers. However when the initial configuration and final MS packing are close together (*i.e.* small l), the fact that the rattler is not always in the same position in the final MS packing leads to a significant error in measuring l and hence $f_n^\Gamma(l)$, as shown in Fig 11. For our measurements of basin volumes at small l , such as V_n^c in Fig. 6, we show results using method 1. Our main results are insensitive to the presence of rattler particles because MS packing probabilities (generated from initially dilute configurations) are determined by features of $f_n^\Gamma(l)$ at large l .

-
- [1] G. Y. Onoda and E. G. Liniger, *Phys. Rev. Lett.* **64** (1990) 2727.
- [2] S. Torquato, T. M. Truskett, and P. G. Debenedetti, *Phys. Rev. Lett.* **84** (2000) 2064.
- [3] E. R. Nowak, J. B. Knight, E. Ben-Naim, H. M. Jaeger, and S. R. Nagel, *Phys. Rev. E* **57** (1998) 1971.
- [4] P. Richard, M. Nicodemi, R. Delannay, P. Ribière, and D. Bideau, *Nature Materials* **4** (2005) 121.
- [5] T. S. Majmudar and R. P. Berhinger, *Nature* **435** (2005) 1079.
- [6] G. R. Farrell, K. M. Martini, and N. Menon, *Soft Matter* **6** (2010) 2925.
- [7] K. L. Johnson, *Contact Mechanics* (Cambridge University Press, New York, 1987).
- [8] N. Xu, J. Blawdziewicz, and C. S. O'Hern, *Phys. Rev. E* **71** (2005) 061306.
- [9] The density landscape is the surface defined by the minimum specific volume (or inverse packing fraction) allowed for each configuration of hard particles.
- [10] F. H. Stillinger and T. A. Weber, *J. Chem. Phys.* **83** (1985) 4767.
- [11] G.-J. Gao, J. Blawdziewicz, and C. S. O'Hern, *Phys. Rev. E* **74** (2006) 061304.
- [12] G.-J. Gao, J. Blawdziewicz, and C. S. O'Hern, *Phys. Rev. E* **80** (2009) 061303.
- [13] F. H. Stillinger and T. A. Weber, *Science* **225** (1984) 983.
- [14] N. Xu, D. Frenkel, A.J. Liu, *Phys. Rev. Lett.* **106** (2011) 245502.
- [15] G. Carlsson, J. Gorham, M. Kahle, and J. Mason, "Computational topology for configuration spaces of hard disks," to appear in *Physical Review E* (2012).
- [16] G.-J. Gao, J. Blawdziewicz, and C. S. O'Hern, *Phys. Rev. E* **80** (2009) 061303.
- [17] T. Aste and T. Di Matteo, *Phys. Rev. E* **77** (2008) 021309.
- [18] F. Lechenault, F. da Cruz, O. Dauchot, and E. Bertin, *J. Stat. Mech.* (2006) P07009.
- [19] A. Panaitescu and A. Kudrolli, *Phys. Rev. E* **81** (2010) 060301(R).
- [20] C. S. O'Hern, L. E. Silbert, A. J. Liu, and S. R. Nagel, *Phys. Rev. E* **68**, 011306 (2003).
- [21] A. Donev, S. Torquato, and F. H. Stillinger, *Phys. Rev. E* **71** (2005) 011105.